CSIRO PUBLISHING

Australian Journal of Physics

Volume 52, 1999

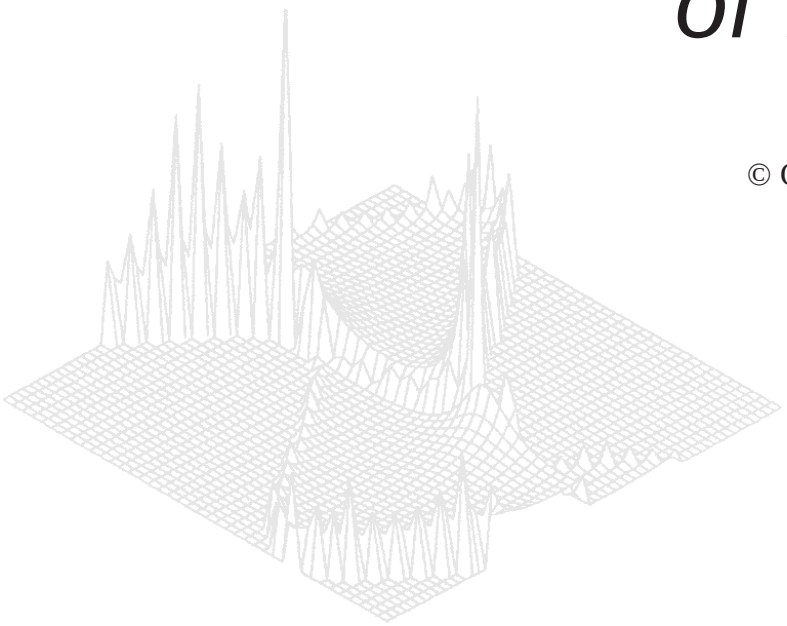

A journal for the publication of
original research in all branches of physics

www.publish.csiro.au/journals/ajp

All enquiries and manuscripts should be directed to
Australian Journal of Physics
CSIRO PUBLISHING
PO Box 1139 (150 Oxford St)
Collingwood Telephone: 61 3 9662 7626
Vic. 3066 Facsimile: 61 3 9662 7611
Australia Email: peter.robertson@publish.csiro.au

Published by **CSIRO** PUBLISHING
for CSIRO Australia and
the Australian Academy of Science

Aust. J. Phys., 1999, **52**, 255–68

Magnetic Phase Diagram for Bilayer Manganites*

Yutaka Moritomo

Centre for Integrated Research in Science and Engineering,
Nagoya University, and PRESTO, JST,
Nagoya 464-8601, Japan.

Abstract

Anisotropic magnetic and transport properties as well as magnetic structures have been investigated for single crystals of bilayer manganites $(La_{1-z}Nd_z)_{2-2x}Sr_{1+2x}Mn_2O_7$ as a function of doping level x and averaged ionic radius z of the rare-earth ion. We have derived a global magnetic phase diagram as a function of x and z. The ferromagnetic metallic state observed in $La_{1\cdot2}Sr_{1\cdot8}Mn_2O_7$ ($x = 0\cdot4$ and $z = 0\cdot0$) is replaced by a layered antiferromagnetic state beyond $x \geq 0\cdot45$. The phase diagram thus obtained is compared with that for the cubic manganites $(La_{1-z}Nd_z)_{1-x}Sr_xMnO_3$.

1. Introduction

The doped manganites $R_{1-x}Sr_xMnO_3$ (R is a trivalent rare-earth atom) with cubic perovskite structure show a variety of physical properties, including the 'colossal' magnetoresistance effect (CMR) (Jin *et al.* 1994) near the insulator-to-metal transition temperature. The generic behaviour of the paramagnetic insulator to ferromagnetic metal transition near T_C is understood within the framework of double-exchange theory (Anderson and Hasagawa 1955; de Gennes 1960), which includes only the transfer integral t of the e_g electrons and the on-site exchange interaction (Hund rule coupling; J_H) between the itinerant e_g electrons and localised t_{2g} spins ($S = \frac{3}{2}$). The magnetoresistive behaviour, especially for $La_{1-x}Sr_xMnO_3$ (Urushibara *et al.* 1995) having a large one-electron bandwidth W of the e_g electrons, is well accounted for by the simple DE model (Furukawa 1994, 1995). Another remarkable feature of the cubic manganites with distorted $GdFeO_3$ structure is that the magnitude of W can be controlled by replacement of the rare-earth ions R^{3+} (chemical pressure effect): by changing the average ionic radius r_A of the perovskite A site, the Mn–O–Mn bond angle and hence W decreases (Radaelli *et al.* 1997; Hwang *et al.* 1995; Fontcuberta *et al.* 1996; Garcvia-Munoz *et al.* 1997). The doped manganites show more multifarious properties in the heavily-doped region ($x \geq 0\cdot5$). For example, $Nd_{0\cdot5}Sr_{0\cdot5}MnO_3$ ($x = 0\cdot5$) shows a charge-ordering (CO) transition at T_{CO}=160 K (Kuwahara *et al.* 1995) accompanying a steep rise of resistivity and a FM-to-AFM transition. Kawano *et al.* (1997) have performed neutron diffraction measurements

* Refereed paper based on a contribution to the International Workshop on the Colossal Magnetoresistance (CMR) Effect, held at the University of Melbourne, 8–11 June 1998.

 10.1071/PH98045 0004-9506/99/020255$05.00

on $Nd_{1-x}Sr_xMnO_3$ and found that the low temperature spin structure changes from CE-type at $x = 0{\cdot}5$ to A-type at $x = 0{\cdot}55$. Recently, Akimoto *et al.* (1998) and Moritomo *et al.* (1998*a*, 1998*b*) have systematically investigated the ground state properties for cubic-type manganites as a function of x and W, and found that the phase diagram is dominated by the FM metallic state in the low-x region and an AFM metallic state in the high-x region.

The Ruddeles–Popper family of doped manganites, $(La, Sr)_{n+1}Mn_nO_{3n+1}$ (n=1, 2 and ∞), has been attracting intensive interest due to their unique crystal structure: the MnO_2 sheets are separated by the rock-salt layers and the MnO_6 octahedra form a two-dimensional (2D) network. The $n = 2$ compound ($La_{1\cdot2}Sr_{1\cdot8}Mn_2O_7$; $x = 0{\cdot}4$) shows the insulator–metal transition accompanying a large magnetoresistance (Moritomo *et al.* 1996). Up to present, extensive studies on the lattice and magnetic structure were performed on $La_{2-2x}Sr_{1+2x}Mn_2O_7$ (Mitchell *et al.* 1997; Akimoto *et al.* 1999; Moritomo *et al.* 1999*a*, 1999*b*; Kubota *et al.* 1999). In this system, the hole-doping procedure not only decreases the nominal concentration of the e_g carriers, but significantly releases the static Jahn–Teller (JT) distortion of the MnO_6 octahedra (Moritomo *et al.* 1998*a*, 1998*b*): the averaged JT distortion Δ defined by $\langle d_{Mn-O(out)}\rangle/d_{Mn-O(in)}$ decreases from $\Delta = 1{\cdot}03$ at $x = 0{\cdot}3$ to $1{\cdot}00$ at $x = 0{\cdot}5$. Such a variation of the JT distortion should affect the orbital character of the e_g electrons, and hence the magnetotransport properties. Moritomo *et al.* (1998*a*, 1998*b*) have investigated the ground state properties for $(La_{1-z}Nd_z)_{2-2x}Sr_{1+2x}Mn_2O_7$ ($x = 0{\cdot}4 - 0{\cdot}5$) by systematically changing z and x, and have found that the $x \geq 0{\cdot}45$ region is dominated by a layered AFM (A-type AFM) state. In this magnetic structure, an FM MnO_2 sheet alternates along the c-axis (intra-bilayer coupling is *negative*) (Moritomo *et al.* 1989*a*, 1998*b*, 1999*a*, 1999*b*). Such a magnetic structure is interpreted in terms of the formation of the pseudo two-dimensional (2D) $d_{x^2-y^2}$ band, which causes the FM double-exchange interaction (Anderson and Hasagawa 1955) within the MnO_2 sheet and AFM superexchange coupling between the adjacent sheets (within the bilayer).

Similar to the case of hole doping, the substitution of the smaller Nd^{3+} ions for the La^{3+} ions (*chemical pressure*) significantly influences the magnetotransport properties of the bilayer manganites. For example, the FM metallic state at $x = 0{\cdot}4$ disappears when the Nd^{3+} concentration (z) exceeds 40% (Moritomo *et al.* 1997). Such a chemical pressure effect has been ascribed to the enhanced static JT distortion and the resultant change of the orbital character of the e_g electrons from $d_{x^2-y^2}$ like to $d_{3z^2-y^2}$ like. Thus, application of chemical pressure for bilayer manganites can be regarded as control of the orbital character of the e_g electrons, making a sharp contrast with that for the cubic manganites.

In this paper, we report anisotropic magnetic and transport properties as well as magnetic structures for bilayer maganites, $(La_{1-z}Nd_z)_{2-2x}Sr_{1+2x}Mn_2O_7$, as a function of nominal hole concentration x and Nd concentration z. We have derived a global magnetic phase diagram as a function of x and z. Such a phase diagram is indispensable *to optimise the magnetoresistive property and to explore a new functionality* of the bilayer manganites. The format of the present paper is as follows. After describing the crystal growth procedure in Section 2, we survey the overall features of the x- and z dependence of the lattice parameters (Section 3*a*). Then, we discuss the filling-dependent magnetotransport properties

for the La- and Nd-based compounds (Section 3*b*). Section 3*c* is devoted to the chemical pressure effects on bilayer manganites and Section 3*d* to magnetic structures. In Section 3*e*, we derive the ground state phase diagram for bilayer manganites as a function of x and z, and argue it in terms of variation of the orbital character of the e_g electrons. A summary is given in Section 4.

2. Experimental

Single crystals of $(La_{1-z}Nd_z)_{1-2x}Sr_{1+2x}Mn_2O_7$ were grown by the floating-zone method at a feeding speed of 20 mm/h. Stoichiometric mixtures of commercial La_2O_3, Nd_2O_3, $SrCO_3$ and Mn_3O_4 powder were ground and calcined twice at 1300°C for 24 h. The resulting powder was pressed into a rod with a size of 5 mmϕ×100 mm and sintered at 1350°C for 48 h. The ingredient could be melted congruently in a flow of oxygen or air. Large single crystals were obtained with two well-defined facets, which correspond to the crystallographic *ab*-plane. For four-probe resistivity measurements, the crystal was cut into a rectangular shape, typically of 3×2×1 mm^3, and electrical contacts were made with a heat-treatment-type silver paint. Susceptibility (magnetisation) was measured under a field of $\mu_0 H = 10$ mT (0·5 T) using a superconducting quantum interference device (SQUID) magnetometer after cooling down to 5 K in the zero field (ZFC).

Powder X-ray diffraction measurements at room temperature and Rietveld analysis (Kim and Izumi 1994) indicated that the crystals were nearly single phase. The crystal symmetry is tetragonal ($I4/mmm$; $Z = 2$) over the whole concentration range. To investigate the magnetic structure, neutron powder diffraction measurements were performed with the Kinken Powder Diffractometer (KPD) for high efficiency and high resolution measurements, and HERMES (Ohoyama *et al.* 1998) installed at the JRR-3M reactor at the Japan Atomic Energy Research Institute, Tokai, Japan. Neutrons with wavelength 1·819 Å were obtained by the (331) reflection of a Ge monochrometer, and 12′-∞-Sample-18′ collimation. Melt-grown crystal ingots were crushed into fine powder and were sealed in a vanadium capsule with helium gas, and mounted at the cold head of the closed-cycle He-gas refrigerator.

3. Results and Discussion

(3a) Overall Feature of the Lattice Parameters

Lattice constants a and c, obtained from the X-ray powder diffraction measurements, are shown in Fig. 1 and Table 1. The upper two panels of Fig. 1 are for the chemical substitution effect (constant x), while the lower panels are for the filling-dependence (constant z). In the case of $x = 0{\cdot}4$ (upper left panel), the lattice constant a steeply decreases with increasing z. Akimoto *et al.* (1998) have performed neutron powder diffraction measurements on $(La_{1-z}Nd_z)_{1\cdot2}Sr_{1\cdot8}Mn_2O_7$ ($z = 0{\cdot}0$, $0{\cdot}2$ and $0{\cdot}4$) at 300 K and determined the distortion of the MnO_6 octahedra; they observed enhancement of the average JT distortion Δ with z. They further calculated the Madelung potential for the $d_{x^2-y^2}$ and $d_{3z^2-r^2}$ orbitals, and found that the enhanced JT distortion stabilises the $d_{3z^2-r^2}$ orbital. On the other hand, the hole-doping procedure (increasing x) considerably shrinks c in both the La (lower left panel) and Nd (lower right panel) compound. Kubota *et al.* (1998) have performed systematic

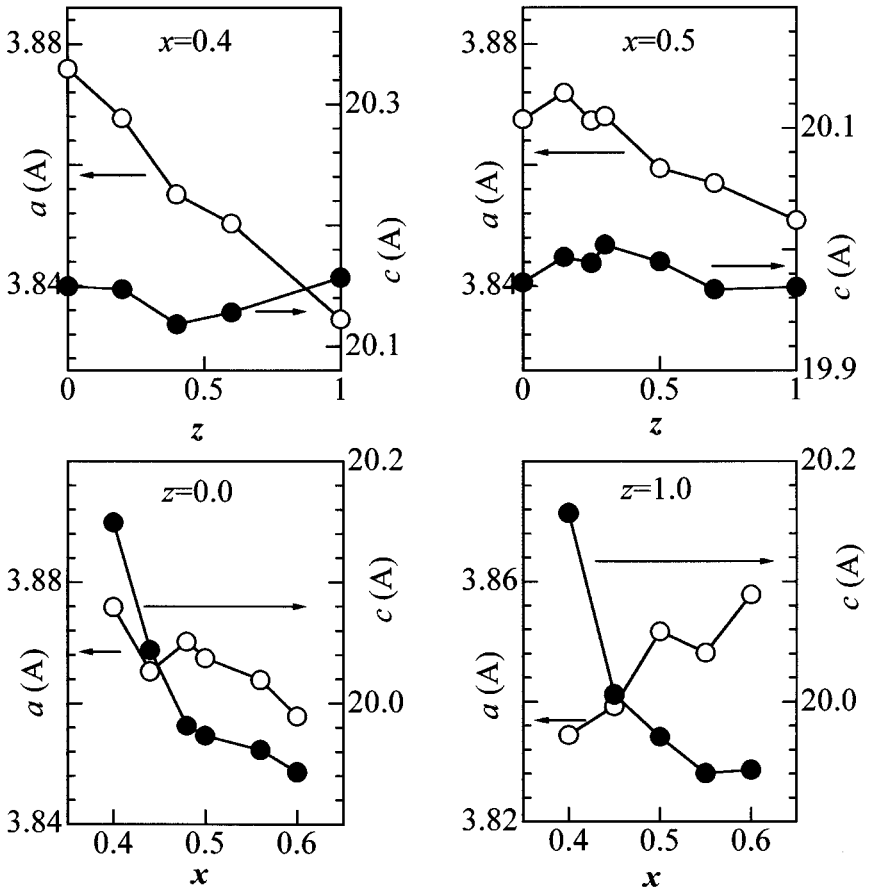

Fig. 1. Lattice constants for $(La_{1-z}Nd_z)_{2-2x}Sr_{1+2x}Mn_2O_7$. Open and solid circles stand for a and c respectively.

Table 1. Lattice constants for $(La_{1-z}Nd_z)_{2-2x}Sr_{1+2x}Mn_2O_7$ at 300 K

x	z	a (Å)	c (Å)	c/a
0·40	1·00	3·8345(2)	20·1569(9)	5·257
0·40	0·60	3·8503(3)	20·1283(8)	5·228
0·40	0·40	3·8551(3)	20·1183(8)	5·219
0·40	0·20	3·8677(2)	20·1472(7)	5·209
0·40	0·00	3·8759(3)	20·1496(9)	5·199
0·44	0·00	3·8653(5)	20·044(1)	5·186
0·45	1·00	3·8393(4)	20·006(1)	5·211
0·48	0·00	3·8702(5)	19·9814(9)	5·163
0·50	1·00	3·8517(3)	19·9708(8)	5·185
0·50	0·70	3·8569(5)	19·967(1)	5·177
0·50	0·50	3·8594(5)	19·9909(8)	5·180
0·50	0·30	3·8680(6)	20·004(1)	5·177
0·50	0·25	3·8673(4)	19·989(1)	5·168
0·50	0·15	3·8719(3)	19·9938(6)	5·164
0·50	0·00	3·8675(6)	19·9732(8)	5·164

structural investigations on $La_{2-2x}Sr_{1+2x}Mn_2O_7$ ($x = 0{\cdot}30$, $0{\cdot}40$, $0{\cdot}45$, $0{\cdot}48$, $0{\cdot}50$), and found significant release of the average JT distortion with x. These experimental facts suggest that the orbital character of the e_g electrons changes from $d_{3z^2-r^2}$ like to $d_{x^2-y^2}$ like with an increase of x or with a decrease of z. Such a variation of the e_g electron character should significantly affect the magnetotransport properties.

We should mention that there are two independent sites within which rare-earth (Nd^{3+} and La^{3+}) or alkaline (Sr^{2+}) earth ions can be distributed, i.e. the twelve-coordinate site [P-site; at (0,0,1/2)] and the nine-coordinate site [R-site; (0,0,z)]. Seshadri *et al.* (1996) have performed Rietveld analysis on the X-ray diffraction patterns for $R_{1\cdot2}Sr_{1\cdot8}Mn_2O_7$ (R =La, Pr and Nd) and shown that the smaller rare-earth ions Nd^{3+} prefer to occupy the R-site (within the bilayer). Such a preference for the occupancy of smaller ions in the rock-salt layer would deform the MnO_6 octahedron, and especially elongate the apical Mn–O bond. Such an effect seems to be crucial in $La_{1\cdot2}(Ca_{1-y}Sr_y)_{1\cdot8}Mn_2O_7$ (Akimoto *et al.* 1998), in which significant elongation of the apical Mn–O bond has been observed. On the other hand, Battle *et al.* (1996, 1997) insisted that some high-x bilayer compounds, e.g. $LaSr_2Mn_2O_7$ and $NdSr_2Mn_2O_7$, are biphase based on their

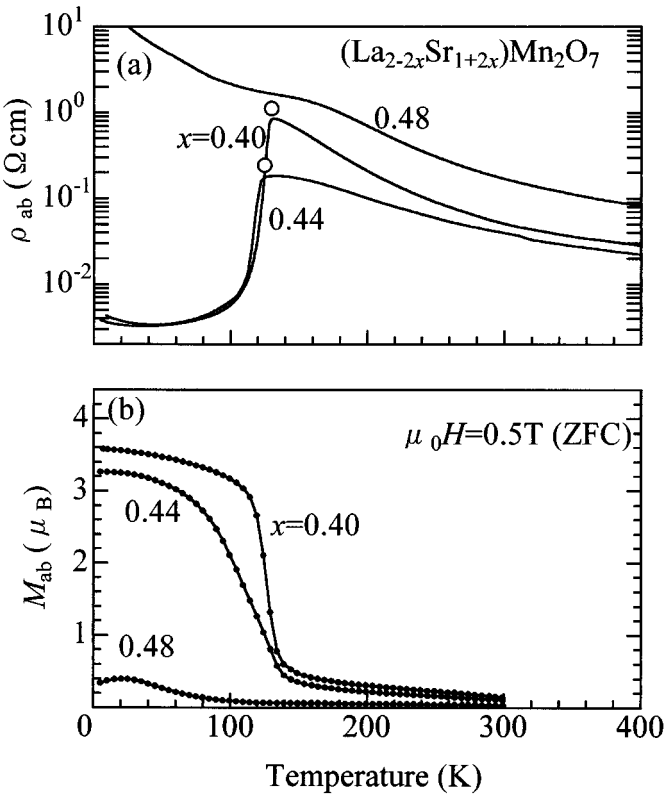

Fig. 2. In-plane component of (a) the resistivity ρ_{ab} and (b) the magnetisation M_{ab} for crystals of $La_{2-2x}Sr_{1+2x}Mn_2O_7$ ($z = 0{\cdot}0$) with variation of x. The open circles indicate the FM transition.

Rietveld analysis of neutron powder profiles of ceramics samples. However, our samples are the melt-grown crystals, and they are expected to be qualitatively better than the ceramic samples. We are now planning to perform high-resolution synchrotron-radiation X-ray diffraction experiments on our melt-grown crystals, which will resolve the above-mentioned problems, i.e. the preference for occupancy as well as the secondary phase.

(3b) Filling Dependence of Magnetotransport Properties

Let us survey the filling dependence of the magnetotransport properties for bilayer manganites. Fig. 2 shows the in-plane component of (a) the resistivity ρ_{ab} and (b) the magnetisation M_{ab} for $La_{2-2x}Sr_{1+2x}Mn_2O_7$. $La_{1\cdot2}Sr_{1\cdot8}Mn_2O_7$ (Moritomo *et al.* 1996) ($x = 0\cdot4$; $z = 0\cdot0$) shows insulating behaviour at room temperature, but is transformed into the FM metallic state below $T_C = 130$ K (see the open circle). The FM transition is suppressed with x, and disappears above $x = 0\cdot48$. Recent detailed neutron diffraction experiments (Hirota *et al.* 1998; Kubota *et al.* 1999) have revealed that the low-temperature magnetic structure changes from FM, canting to AFM with an increase of x. At $x = 0\cdot48$, the compound is of A-type AFM ($T_N \approx 200$ K), in which the FM MnO_2 sheet

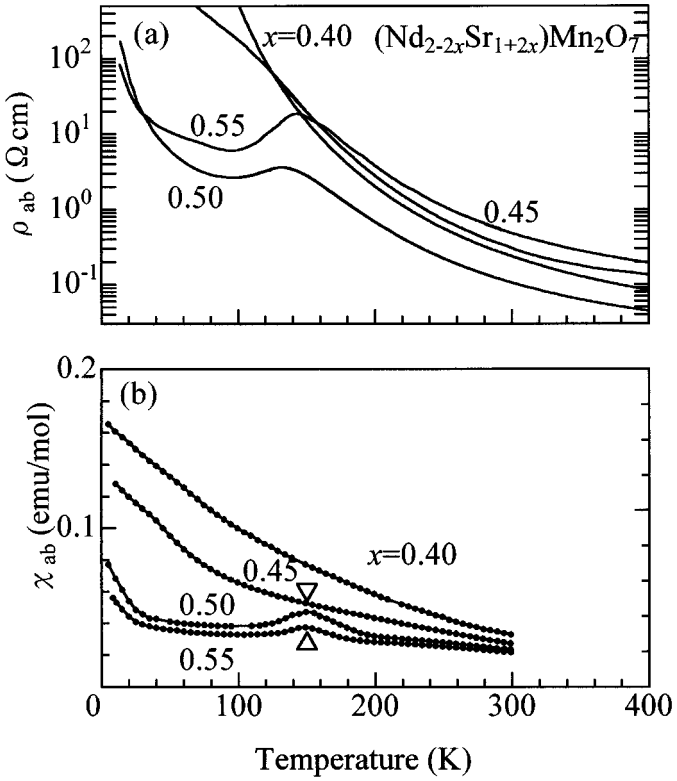

Fig. 3. In-plane component of (a) the resistivity ρ_{ab} and (b) the susceptibility χ_{ab} for crystals of $Nd_{2-2x}Sr_{1+2x}Mn_2O_7$ ($z = 1\cdot0$) with variation of x. The open triangles indicate the AFM transition.

alternates along the c-axis (the intra-bilayer coupling is *negative*; see the schematic picture in Fig. 7), without any FM components. We note that the insulating behaviour in the $\rho_{ab} - T$ curve is slightly suppressed around T_N, which is ascribed to the reduced spin scattering in the spin-ordered AFM phase.

Fig. 3 shows the in-plane component of (a) the resistivity ρ_{ab} and (b) the susceptibility χ_{ab} for $Nd_{2-2x}Sr_{1+2x}Mn_2O_7$. The compound at $x = 0{\cdot}40$ shows an insulating behaviour down to the lowest temperature. The χ_{ab}-T curves at $x = 0{\cdot}50$ and $0{\cdot}55$, however, show an AFM transition at $T_N \approx 150$ K, as indicated by the triangles. Moritomo *et al.* (1999*a*, 1999*b*) have performed neutron diffraction measurements on $NdSr_2Mn_2O_7$ ($x = 0{\cdot}5$), and confirmed that the magnetic structure is the same as that for $LaSr_2Mn_2O_7$. Similar the case of $La_{2-2x}Sr_{1+2x}Mn_2O_7$, the reduction of the ρ_{ab} value is observed around T_N at $x = 0{\cdot}50$ and $0{\cdot}55$.

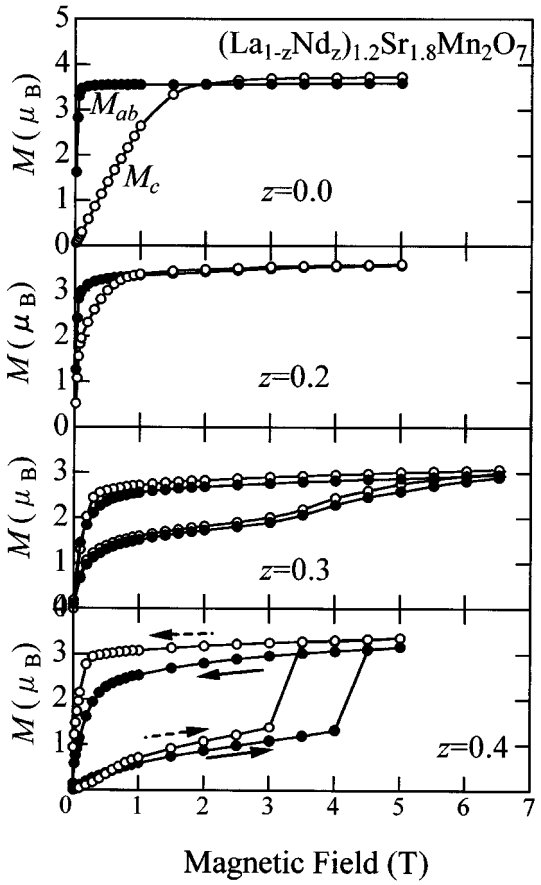

Fig. 4. Magnetisation curves for $(La_{1-z}Nd_z)_{1\cdot2}Sr_{1\cdot8}Mn_2O_7$. The applied magnetic field is either parallel (M_{ab}; solid circles) or perpendicular (M_c; open circles) to the MnO_2 sheet.

(3c) Chemical Pressure Effect on the Magnetic Properties

Now let us proceed to the chemical pressure effect on the magnetic properties. Fig. 4 shows the magnetisation curves for $(La_{1-z}Nd_z)_{1\cdot2}Sr_{1\cdot8}Mn_2O_7$ ($x = 0{\cdot}4$)

at 5 K. For $z = 0{\cdot}0$, the magnetisation curve shows a large anisotropy (e.g. $M_{ab}/M_c \sim 20$ at $\mu_0 H = 10$ mT) in a low field, indicating that the easy axis lies on the MnO_2 sheet. The anisotropy M_{ab}/M_c, however, rapidly decreases to $\sim$2 for $z = 0{\cdot}2$, and almost vanishes for $z = 0{\cdot}4$. The magnetisation curve for $z = 0{\cdot}4$ shows an abrupt jump at $\mu_0 H \approx 4$ T for H parallel to ab and at $\mu_0 H \approx 3$ T for H parallel to c, indicating a paramagnetic-FM metamagnetic transition. In the field-induced FM phase, the easy axis is along the c-direction, in sharp contrast to the case for $z = 0{\cdot}0$. The change of the easy axis originated in a variation of the e_g electron character from $d_{x^2-y^2}$ like ($z \leq 0{\cdot}3$) to $d_{3z^2-r^2}$ like ($z \geq 0{\cdot}4$). The magnetisation curves for $z = 0{\cdot}6$ and $1{\cdot}0$ (not shown) continue increasing beyond 5 T, showing a paramagnetic behaviour.

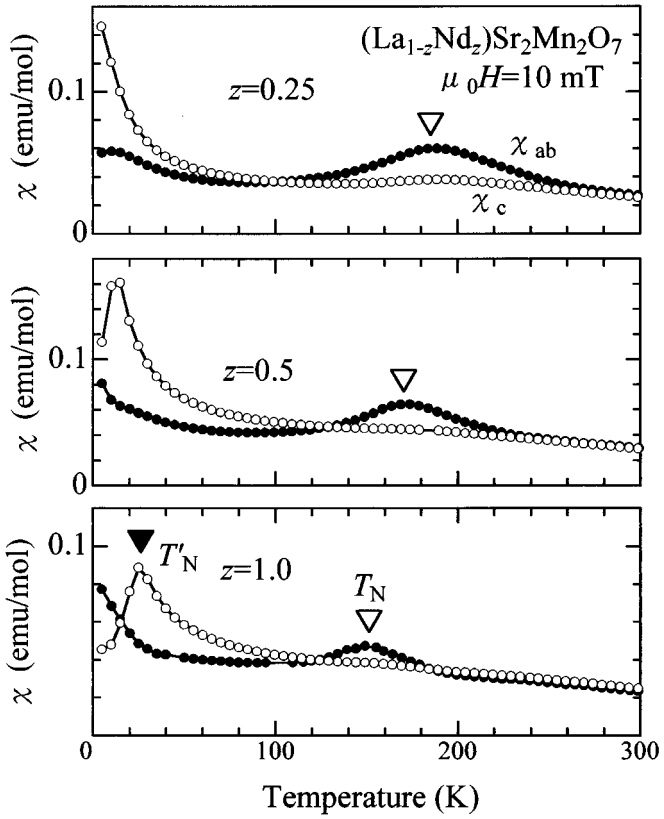

Fig. 5. Susceptibility for $(La_{1-z}Nd_z)Sr_2Mn_2O_7$. The applied magnetic field is either parallel (χ_{ab}; solid circles) or perpendicular (χ_c; open circles) to the MnO_2 sheet. The triangles indicate AFM phase transitions (see text). The susceptibilities were measured after cooling down to 5 K in a zero field.

In contrast to the case for $x = 0{\cdot}4$, the chemical pressure effect is not so significant for $= 0{\cdot}5$. Fig. 5 shows the anisotropic magnetic susceptibility for $(La_{1-z}Nd_z)Sr_2Mn_2O_7$. The χ_{ab} value for $NdSr_2Mn_2O_7$ (lowest panel) shows a drop at $T_N \approx 150$ K (see the open triangle) due to the AFM phase transition. An anomaly in the χ_c–T curve at $T'_N \approx 30$ K (solid triangle) is due to rotation of the

Mn moments from an in-plane direction to an out-of-plane direction (Moritomo *et al.* 1999*a*, 1999*b*; Battle *et al.* 1996). Chemical substitution of larger La^{3+} ions for Nd^{3+} ions does not alter the overall features of the χ–T curves, but a shift of T_N and T_N'; with increasing z, T_N gradually decreases from 180 K at $z = 0{\cdot}25$ to ~ 150 K at $z = 1{\cdot}0$. Significant suppression of T_N' with dilution of the Nd^{3+} ion (a decrease in z) implies that the AFM–AFM transition is triggered by ordering of the Nd^{3+} ions (Battle *et al.* 1996). Such a small chemical pressure effect is considered to reflect the stability of the $d_{x^2-y^2}$ like orbital due to the released JT distortion (see Section 3*a*) over the concentration range ($0{\cdot}25 \leq z \leq 1{\cdot}00$ and $x = 0{\cdot}5$). In fact, the averaged JT distortion is $\Delta = 1{\cdot}01$ even for $NdSr_2Mn_2O_7$ ($z = 1{\cdot}0$), which is smaller than the value for $La_{1{\cdot}2}Sr_{1{\cdot}8}Mn_2O_7$ ($\Delta = 1{\cdot}02$) (Moritomo *et al.* 1998*a*, 1998*b*).

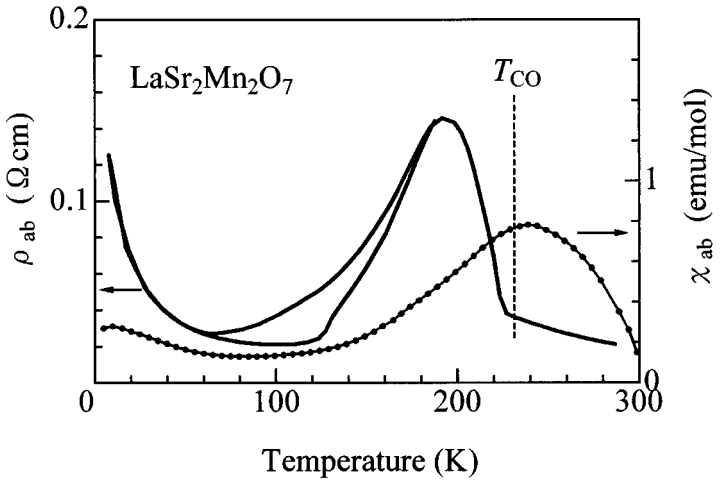

Fig. 6. In-plane components of resistivity ρ_{ab} (thick curve) and susceptibility χ_{ab} (solid circles) for $LaSr_2Mn_2O_7$. The susceptibilities were measured after cooling down to 5 K in a zero field. Here T_{CO} means the critical temperature for the charge-ordering transition.

The magnetotransport properties becomes singular at $z = 1{\cdot}0$ ($LaSr_2Mn_2O_7$; see Fig. 6). The χ_{ab}–T curve begins to decrease below $T_{CO} \approx 230$ K accompanying a steep rise of the in-plane component of resistivity ρ_{ab}. Such a steep rise in resistivity can be ascribed to the charge-ordering transition. Li *et al.* (1998) have performed electron diffraction measurements on $LaSr_2Mn_2O_7$, and found four-fold superlattice reflections; they proposed that in-plane ordering of the $d_{3x^2-r^2}$ and $d_{3y^2-r^2}$ orbitals is accompanied by the charge-ordering transition at $T_{CO} \approx 230$ K. A similar rise of ρ_{ab} and suppression of χ_{ab} is observed in the single-layered compound $La_{0{\cdot}5}Sr_{1{\cdot}5}MnO_4$ (Moritomo *et al.* 1995; Murakami *et al.* 1998; Bao *et al.* 1996; Sternlieb *et al.* 1996). With a further decrease in temperature below T_{CO}, however, the ρ_{ab} value decreases, accompanying a prominent thermal-hysteresis. Such reentrant behaviour indicates melting of the charge-ordered state below ~ 100 K (Moritomo *et al.* 1999*a*, 1999*b*; Kimura *et al.* 1996). Consistently with this, the low temperature magnetic structure for $LaSr_2Mn_2O_7$ is the same as that for $NdSr_2Mn_2O_7$, making a sharp contrast with

the CE-like structure observed in $La_{0\cdot5}Sr_{1\cdot5}MnO_4$ (Sternlieb *et al.* 1996). The appearance of the charge-ordered state in the limited z region around $z = 1\cdot0$ can be ascribed to the released JT distortion. The Δ value is $1\cdot00$ at $z = 1\cdot0$ (Moritomo *et al.* 1998*a*), but becomes larger with a decrease in z ($\Delta = 1\cdot01$ for $z = 1\cdot0$). As Li *et al.* (1998) proposed, the charge-ordered state in this system is considered to be stabilised by concomitant orbital ordering within the MnO_2 sheet. For $z = 1\cdot0$ with smaller JT distortion along the c-axis, the charge- and orbital-ordered state is easily realised. With decreasing z, however, the orbital-ordered state within the MnO_2 sheet is difficult to obtain, since the e_g electrons are dominated by the $d_{3z^2-r^2}$ character. Similarly, in single-layer manganites $R_{0\cdot5}Sr_{1\cdot5}MnO_4$ (R =$Nd_{1-z}La_z$) (Moritomo *et al.* 1997*a*, 1997*b*), enhanced JT distortion destabilises the charge ordering by variation of the orbital character of the e_g electrons.

(3d) Magnetic Structures

Fig. 7 shows schematically the low-temperature magnetic structures determined by Rietveld analysis on the neutron powder patterns. $La_{1\cdot2}Sr_{1\cdot8}Mn_2O_7$ ($x = 0\cdot4$ and $z = 0\cdot0$) is FM with easy axis along the in-plane direction (see also the uppermost panel of Fig. 4) (Mitchell *et al.* 1997; Hirota *et al.* 1998; Kubota *et al.* 1999*a*, 1999*b*). For $La_{1\cdot4}Sr_{1\cdot6}Mn_2O_7$ ($x = 0\cdot3$), enhanced static JT distortion ($\Delta = 1\cdot03$) raises the local t_{2g} spins along the c-direction (Kubota *et al.* 1999*a*, 1999*b*; Moritomo and Itoh 1999). A similar variation of the easy

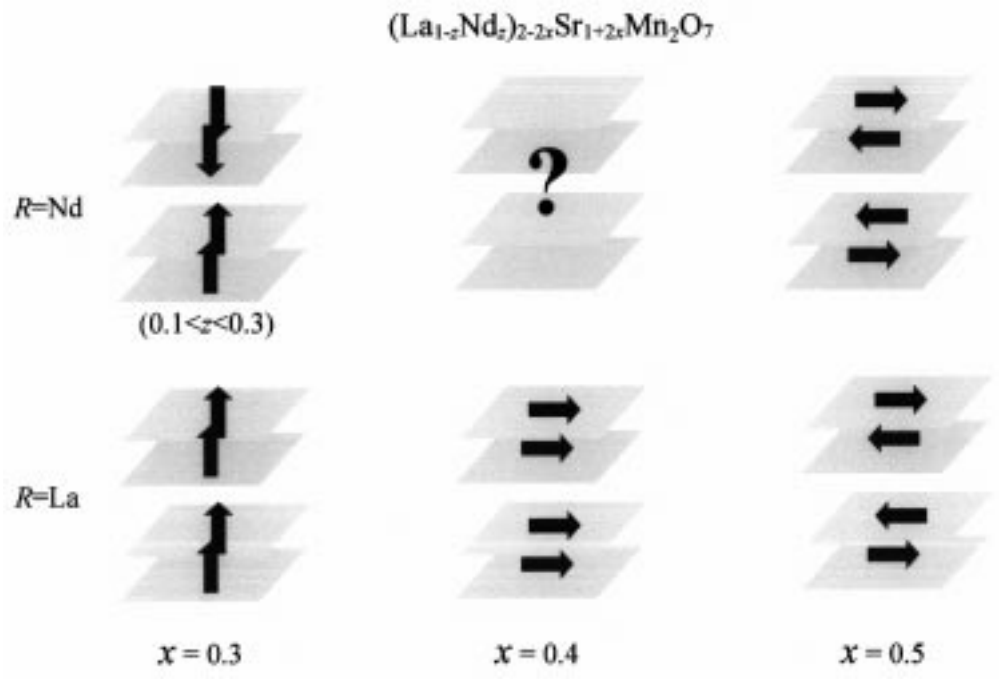

Fig. 7. Schematic magnetic structure for $(La_{1-z}Nd_z)_{2-2x}Sr_{1+2x}Mn_2O_7$ determined from neutron powder diffraction measurements. The parallelograms represent the respective MnO_2 sheets.

axis is observed in the field-induced FM state of $(La_{0.6}Nd_{0\cdot4})_{1\cdot2}Sr_{1\cdot8}Mn_2O_7$ ($x = 0\cdot4$ and $z = 0\cdot4$; see the lowest panel of Fig. 4). The FM state at $x = 0\cdot3$ is fairly unstable, and a slight substitution (10–30%) of the Nd^{3+} ion changes the ground state from FM to AFM (Moritomo *et al.* 1999*a*, 1999*b*). As seen from the schematic picture in Fig. 7, the magnetic structure for the $x = 0\cdot3$ system is governed by the weak coupling *between the bilayers*. We further observed field-induced AFM–FM metamagnetic behaviour in $(La_{0\cdot9}Nd_{0\cdot1})_{1\cdot4}Sr_{1\cdot6}Mn_2O_7$ as well as concomitant spin-valve magnetoresistance in the current perpendicular to the plane (CPP) configuration (Moritomo and Itoh 1999; Moritomo *et al.* 1999*a*, 1999*b*). We think that this is the origin of the low-filled magnetoresistance observed in $La_{1.4}Sr_{1\cdot6}Mn_2O_7$ ($x = 0\cdot3$) (Kimura *et al.* 1996).

In the high-x compounds, e.g. $LaSr_2Mn_2O_7$ and $NdSr_2Mn_2O_7$, the magnetic structure is of A-type AFM: ferromagnetic within the MnO_2 sheet but antiferromagnetic between the neighbouring sheets (Moritomo *et al.* 1999*a*, 1999*b*; Battle *et al.* 1996). The AFM structure at $x = 0\cdot5$ originates in the negative coupling *within the bilayer*, making a sharp contrast with the case at $x = 0\cdot3$. The same structure has been observed for $La_{1\cdot2}(Sr_{0\cdot6}Ca_{0\cdot4})_{1\cdot8}Mn_2O_7$ ($x = 0\cdot4$) (Akimoto *et al.* 1999), suggesting that the structure is fundamental for bilayer manganites. We have further measured powder profiles for $(La_{0\cdot6}Nd_{0\cdot4})_{1\cdot2}Sr_{1\cdot8}Mn_2O_7$ ($x = 0\cdot4$ and $z = 0\cdot4$), and observed a slight trace of the A-type AFM component. The magnetic moment obtained is, however, small ($0\cdot5\pm0\cdot05\mu_B$) compared with the ideal value ($=3\cdot5\ \mu_B$). Therefore, we think that the AFM component is not intrinsic, but due to some secondary phase or phase segregation.

(3e) Ground State Phase Diagram

We summarise in Fig. 8 the ground state properties thus obtained for bilayer manganites in the xz plane. The solid circles and triangles represent the FM and A-type AFM phase respectively. Open triangles mean that the exact magnetic structure is unknown (see Section 3*d*). The most important message of the phase diagram is that the ground state changes from the FM to the A-type AFM state with hole-doping beyond $x \sim 0\cdot45$. Such a global feature of the ground state phase diagram in the $x = 0\cdot4 - 0\cdot5$ region bares a close resemblance with that for the cubic manganites. Fig. 9 shows the phase diagram for $(La_{1-z}Nd_z)_{1-x}Sr_xMnO_3$ (cited in Akimoto *et al.* 1998), in which the layered-AF state appears in the heavily-doped region ($\geq 0\cdot45$).

The key factor that realises the A-type AFM state is considered to be the anisotropy of the two e_g orbitals, i.e. the two-dimensional $d_{x^2-y^2}$ state and the one-dimensional $d_{3z^2-r^2}$ state. In the heavily-doped region, the e_g electron system gains the maximum kinetic energy when the $d_{x^2-y^2}$ orbitals form a pseudo-2D band (Maezono *et al.* 1998). The reduced static JT distortion in the high-x region is also advantageous for such a band structure. If such a $d_{x^2-y^2}$ band were realised, the in-plane exchange interaction would be FM mediated by the itinerant $d_{x^2-y^2}$ electrons (double-exchange interaction), while the AFM superexchange interaction would dominate along the z-direction. This can explain not only the A-type spin structure, but also the reduction of the ρ_{ab} value below T_N (see Fig. 4*a*). With a decrease of x, however, the A-type AFM state changes into the FM state. One probable cause that destroys the $d_{x^2-y^2}$ band is the increasing static JT distortion of the MnO_6 octahedra (see Section 3*a*), which stabilises the

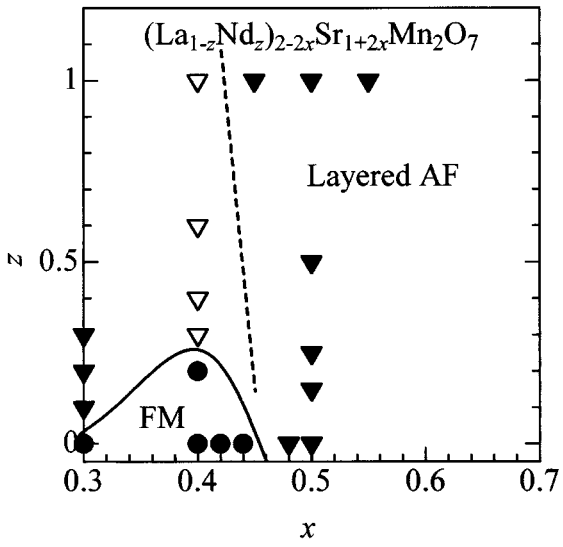

Fig. 8. Ground states for $(La_{1-z}Nd_z)_{2-2x}Sr_{1+2x}Mn_2O_7$ as a function of nominal hole concentration x and Nd concentration z. The solid circles and triangles represent the FM metallic and A-type AFM states respectively. The open triangles mean that the exact magnetic structure is unknown (see text).

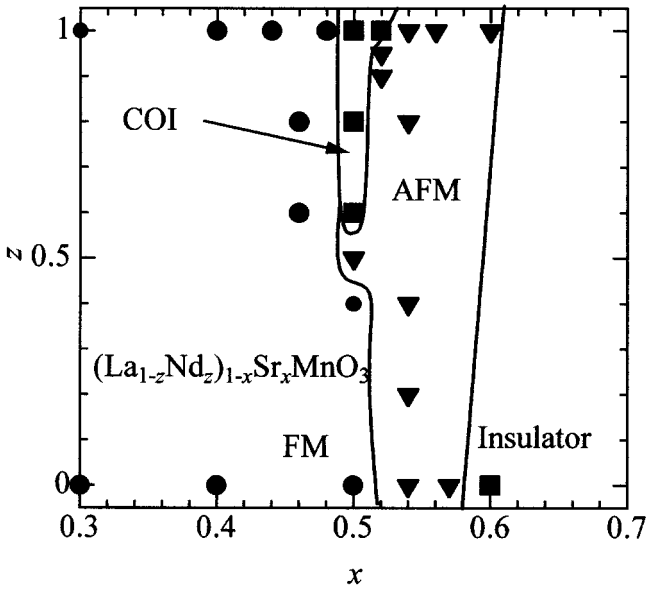

Fig. 9. Ground states for $(La_{1-z}Nd_z)_{1-x}Sr_xMnO_3$ as a function of nominal hole concentration x and Nd concentration z. The circles, triangles and squares represent the FM metallic, AFM metallic, and insulating states respectively. The charge-ordered insulating (COI) state is indicated.

one-dimensional $d_{3z^2-r^2}$ state. Nevertheless, the similarity of the phase diagrams for the bilayer and cubic systems strongly suggests that the doping-level (=1−x) is another key factor that determines the magnetic structure. The increasing doping-level (decreasing x) tends to modify the e_g band structure from pseudo-2D to 3D type to lower the centre of mass for the occupied state (Maezono *et al.* 1998).

Finally, let us comment on the AFM state at $x = 0{\cdot}3$ (see Fig. 7). This AFM structure is governed by the weak negative *inter-bilayer* coupling, making a sharp contrast with the above mentioned A-type AFM state governed by the strong *intra-bilayer* coupling. The origin of the inter-bilayer coupling is rather complicated, compared with the intra-bilayer coupling, due to the larger spacing between the local t_{2g} spins. We believe, however, that the physics for the $x = 0{\cdot}3$ system is qualitatively different from that for the $x = 0{\cdot}4$–$0{\cdot}5$ region, judging from the significantly elongated MnO_6 octahedra (e.g. $\Delta = 1{\cdot}03$ at $x = 0{\cdot}3$ and $z = 0{\cdot}0$) and the resultant stabilisation of the $d_{3z^2-r^2}$ orbital. In order to clarify the physics for the $x = 0{\cdot}3$ system, detailed neutron diffraction experiments on $(La_{1-z}Nd_z)_{1{\cdot}4}Sr_{1{\cdot}6}Mn_2O_7$ are now in progress.

4. Summary

In summary, we have revealed the anisotropic magnetic and transport properties as well as the magnetic structures for single crystals of $(La_{1-z}Nd_z)_{2-2x}Sr_{1+2x}Mn_2O_7$ with bilayer structure as a function of nominal hole concentration x and Nd concentration z. The FM metallic state observed in $La_{1{\cdot}2}Sr_{1{\cdot}8}Mn_2O_7$ ($x = 0{\cdot}4$ and $z = 0{\cdot}0$) disappears with increasing x or z. The phase diagram obtained has a close resemblance with that for the cubic manganites. In both the phase diagrams, the A-type AFM state dominates beyond $x \sim 0{\cdot}45$. We have ascribed the AFM state to a variation in the orbital character of the e_g electrons, and the resultant formation of a pseudo-2D band of the $d_{x^2-y^2}$ orbitals.

Acknowledgments

The author would like to thank K. Hirota, M. Kubota, H. Yoshizawa, K. Ohoyama and M. Ohashi for their help with neutron powder measurements, and Y. Maruyama for his help with crystal preparation. This work was supported by a Grant-in-Aid for Scientific Research from the Ministry of Education, Science, Sports and Culture, and from Precursory Research for Embryonic Science and Technology (PRESTO), Japan Science and Technology Corporation (JST).

References

Akimoto, T., Maruyama, Y., Moritomo, Y., Nakamura, A., Ohoyama, K., Ohashi M., and Hirota, K. (1998). *Phys. Rev.* B **57**, R5594–7.

Akimoto, T., Moritomo, Y., Ohoyama, K., and Ohashi, M. (1999). (in preparation).

Anderson, P. W., and Hasagawa, H. (1955). *Phys. Rev.* **100**, 675–81.

Battle, P. D., Green, M. A., Laskey, N. S., Millburn, J. E., Radaelli, P. G., Rosseinsky, M. J., Sullivan, S. P., and Vente, J. F. (1996). *Phys. Rev.* B **54**, 15967–77.

Battle, P. D., Green, M. A., Laskey, N. S., Milburn, J. E., Murphy, L., Rosseinsky, M. J., Sullivan, S. P., and Vente, J. F. (1997). *Chem. Mater.* **9**, 552–9.

de Gennes, P.-G. (1960). *Phys. Rev.* **118**, 141.

Fontcuberta, J., Maetinez, B., Seffar, Pinol, S., Garcia-Munoz, J. L., and Obradors, X. (1996). *Phys. Rev. Lett.* **76**, 1122–5.

Furukawa, N. (1994). *J. Phys. Soc. Jpn* **63**, 3214–7.
Furukawa, N. (1995). *J. Phys. Soc. Jpn* **64**, 2734–7; 2754–7; 3164–7.
Garcvia-Munoz, J. I., Snaaidi, M., Fontcuberta, J., and Redriguez-Carvajal, J. (1997). *Phys. Rev.* **55**, 34–7.
Hirota, K., Moritomo, Y., Fujioka, H., Kubota, M., Yoshizawa, H., and Endo, Y. (1998). *J. Phys. Soc. Jpn* **67**, 3380–3.
Hwang, H.-Y., Cheong, S.-W., Radaelli, P. G., Marezio, M., and Batlogg, B. (1995). *Phys. Rev. Lett.* **75**, 914–7.
Jin, S., Tiefel, T. H., McCormack, M., Fastnacht, R., Ramesh, R., and Chen, L.-H. (1994). *Science* **264**, 13–6.
Kawano, H., Kajimoto, K., Yoshizawa, H., Tomioka, Y., Kuwahara, H., and Tokura, Y. (1997). *Phys. Rev. Lett.* **78**, 4253–6.
Kimura, T., Tomioka, Y., Kuwahara, H., and Tokura, Y. (1996). *Science* **274**, 1698–701.
Kimura, T., Kumai, R., Tokuta, Y., Li, J. Q., and Matsui, Y. (1998). *Phys. Rev.* B **58**, 11081–4.
Kubota, M., Yoshizawa, H., Hirota, K., Fujioka, M., Endo, Y., and Moritomo, Y. (1999*a*). *J. Phys. Chem. Solids*, in press.
Kubota, M., Yoshizawa, H., Hirota, K., Fujioka, H., Endo, Y., and Moritomo, Y. (1999*b*). in preparation.
Kuwahara, H., Tomioka, Y., Asamitsu, A., Moritomo, Y., and Tokura, Y. (1995). *Science*, **270**, 961–4.
Li, J. Q., Matsui, Y., Kimura, T., and Tokura, Y. (1998). *Phys. Rev.* B **57**, R3205–8.
Maezono, R., Ishihara, S., and Nagaosa, N. (1998). *Phys. Rev.* B **57**, R13993–6; **58**, 11583–96.
Mitchell, J. M., Argyriou, D. N., Jorgensen, J. D., Hinks, D. G., Potter, C. D., and Bader, S. D. (1997). *Phys. Rev.* B **55**, 63–6.
Moritomo, Y., and Itoh, M. (1999). (submitted).
Moritomo, Y., Tomioka, Y., Asamitus, A., and Tokura, Y. (1995). *Phys. Rev.* B **51**, 3297–300.
Moritomo, Y., Asamitsu, A., Kuwahara, H., and Tokura, Y. (1996). *Nature* **380**, 141–4.
Moritomo, Y., Maruyama, Y., Akimoto, T., and Nakamura, A. (1997*a*). *Phys. Rev.* B **56**, R7057–60.
Moritomo, Y., Nakamura, A., Ohoyama, K., and Ohashi, M. (1997*b*). *Phys. Rev.* B **56**, 14879–82.
Moritomo, Y., Akimoto, Y., Nakamura, A., Ohoyama, K., and Ohashi, M. (1998*a*). *Phys. Rev.* B **58**, 5544–9.
Moritomo, Y., Maruyama, Y., Akimoto, T., Nakamura, A. (1998*b*). *J. Phys. Soc. Jpn* **67**, 405–8.
Moritomo, Y., Nakamura, A., Hirota, K., Ohoyama, K., and Ohashi, M. (1999*a*). *J. Phys. Soc. Jpn*, in press.
Moritomo, A., Ohoyama, K., and Ohashi, M. (1999*b*). *Phys. Rev.* B **59**, in press.
Murakami, Y., Kawada, H., Kawata, H., Tanaka, M., Arima, T., Moritomo, Y., and Tokura, Y. (1998). *Phys. Rev. Lett.* **80**, 1932–6.
Ohoyama, K., Kanouchi, K., Nemoto, K., Ohashi, M., Kajitani, T., and Yamanguchi, Y. (1998). *Jpn J. Appl. Phys.* **37**, 3319.
Radaelli, P. G., Iannone, G., Marezio, M., Hwang, H.-Y., Cheong, S.-W., Jorgensen, J. D., and Argyriou, D. N. (1997). *Phys. Rev.* B **56**, 8265–76.
Seshadri, R., Martin, C., Maigna, A., Hervieu, M., Raveau, B., and Rao, C. N. R. (1996). *J. Mater. Chem.* **6**, 1585–90.
Sternlieb, B. J., Hill, J. P., Wildgruber, U. C., Luke, G. M., Nachumi, B., Moritomo, Y., and Tokura, Y. (1996). *Phys. Rev. Lett.* **76**, 2169–72.
Urushibara, A., Moritomo, Y., Arima, T., Asamitsu, A., Kido, G., and Tokura, Y. (1995). *Phys. Rev.* B **51**, 14103–9.

Manuscript received 9 June, accepted 27 November 1998